



ELSEVIER

Applied Surface Science 196 (2002) 250–263

applied
surface science

www.elsevier.com/locate/apsusc

Irreversible adsorption of colloid particles at heterogeneous surfaces

Zbigniew Adamczyk^{*}, Barbara Siwek, Paweł Weroński, Elizeusz Musiał

Institute of Catalysis and Surface Chemistry, Polish Academy of Sciences, 30-239 Kraków, Niezapominajek 8, Poland

Abstract

Irreversible adsorption of colloid particles at heterogeneous surfaces was studied theoretically and experimentally. The substrate surface of controlled heterogeneity was created by covering a homogeneous surface by adsorption sites (active centers) of a desired concentration. The centers were modeled as spheres smaller in size than the adsorbing particles. Adsorption was assumed to occur due to short-ranged attractive interactions if the colloid particle contacted the center. Extensive Monte-Carlo type simulations were performed. This allowed one to determine the initial flux, adsorption kinetics, jamming coverage and the structure of the particle monolayer as a function of the site coverage Θ_s and the particle/site size ratio, λ . It was revealed that the initial flux increased significantly with Θ_s and the λ parameter. This behavior was quantitatively interpreted in terms of the scaled particle theory. It also was demonstrated that particle adsorption kinetics and the jamming coverage increased abruptly, at fixed site coverage, with λ , attaining for $\lambda^2 \Theta_s \gg 1$ the value pertinent to continuous surfaces. The theoretical predictions were tested experimentally using monodisperse colloid particles (negatively charged polystyrene latex) and the direct microscope observation method. The heterogeneous surface was produced by covering mica by positively charged latex particles of smaller dimension. Particle adsorption kinetics was determined as a function of site (small particle) coverage. It was demonstrated, in accordance with theory, that the initial flux attains the limiting value pertinent to homogeneous surfaces for a site coverage of a few percent. In this case adsorption kinetics was well reflected by the random sequential adsorption (RSA) model.

© 2002 Published by Elsevier Science B.V.

Keywords: Adsorption of colloids; Colloid adsorption; Heterogeneous surface adsorption; Irreversible adsorption; Kinetics of particle adsorption; Random site adsorption

1. Introduction

Adsorption and deposition (irreversible adsorption) of colloid particles, proteins and other bio-materials on solid/liquid interfaces is of large significance for many processes such as filtration, paper making, thrombosis, separation of proteins, bacteria, viruses, enzymes, pathological cells, etc. The kinetics of these processes is regulated by the use of coupling agents

bound to interfaces promoting adherence of particles, e.g. polyelectrolytes [1,2]. In biomedical applications, special proteins (ligands) attached to the surface are applied for a selective binding of a desired solute from protein mixtures as is the case in the affinity chromatography [3]. Analogously, in immunological assays [4] one is often using special proteins (antibodies) attached electrostatically or covalently to colloid particles (e.g. polystyrene latex) to promote selective adsorption of other proteins (antigens) present in serum. This leads to aggregation (agglutination) of a colloid suspension which can easily be evidenced experimentally [5].

^{*} Corresponding author. Tel.: +48-12-639-5104;
fax: +48-12-425-1923.
E-mail address: neadamcz@cyf-kr.edu.pl (Z. Adamczyk).

Similarly, many studies on colloid particle adsorption were performed using surfaces modified by polymers, surfactants or chemical coupling agents (silanes) that changed the natural surface charge of substrate surfaces [6,7]. This is often the case with natural mica used as a molecularly smooth substrate in many particle deposition studies [8].

A characteristic feature of these processes is that particle or protein adsorption occurs at surfaces, which are inherently heterogeneous. Despite the significance of particle adsorption at such surfaces, this subject has been studied a little. Some theoretical calculations concerning the initial flux and jamming coverage for heterogeneous surfaces have been reported in [9]. On the other hand, preliminary experimental results derived for mica covered by polystyrene latex particles has been discussed in [10]. These results concerned the initial adsorption stage when the blocking effects of adsorbed particles were negligible.

The goal of this paper is to extend these measurements to the higher particle coverage range which is of great interest from the practical viewpoint. These experiments are interpreted in terms of theoretical predictions derived from Monte-Carlo type simulations.

2. The simulation algorithm

In our model the adsorption sites (surface heterogeneities) are represented by hard spheres of radius a_s (see Fig. 1). There are N_s^0 spheres distributed over a homogeneous surface having the geometrical surface area ΔS . Without loss of generality one can assume $\Delta S = 1$ and normalize accordingly the sphere dimension. The surface concentration (2D density) of the sites is then equal to N_s^0 and the dimensionless coverage is defined as $\Theta_s = \pi a_s^2 N_s^0$. The configuration of sites of a desired coverage was produced via the random sequential adsorption (RSA) process described at length elsewhere [8,11–13]. According to this approach particles were placed at random in a consecutive manner over the simulation area ΔS . If there was no overlapping of the virtual site particle with any previously places sites the adsorption attempt was accepted (the particle was adsorbed at a given position). Otherwise the adsorption attempt was repeated until the desired coverage of site particles

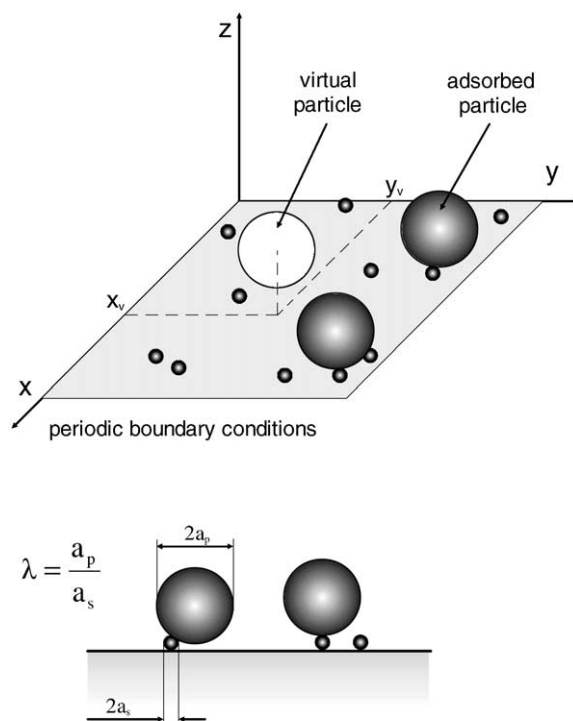


Fig. 1. A schematic representation of particle adsorption modeling over heterogeneous surfaces bearing spherically shaped adsorption sites.

was attained. The heterogeneous surface produced it the RSA process was used in further simulations of colloid particle adsorption. These simulations were carried out in a manner similar to the classical RSA scheme by assuming that particles can only be adsorbed upon touching the site, see Fig. 1. Otherwise at bare interface the particle will not adsorb. Physically, this corresponds to the situation when the particles are irreversibly bound to the sites due to short-ranged attractive interactions of an electrostatic or chemical nature. Furthermore, particle adsorption was assumed irreversible and localised, which means that particle position at the site remained fixed during the entire simulation run.

In accordance with these assumptions, particle adsorption at the heterogeneous surfaces was modeled according to the algorithm:

- (i) An adsorbing (virtual) particle of radius a_p was generated at random within the simulation area covered previously by sites, if it did not touch any

of the sites it was rejected and another virtual particle was produced (the number of attempts N_{att} was increased by one).

- (ii) Otherwise, if the particle touched any of the sites, the overlapping test was performed according to the usual RSA rules, i.e. it was checked if there is any previously adsorbed particle within the exclusion volume (see Fig. 1), if there was overlapping the simulation loop was repeated (the number of attempts was increased by one).
- (iii) If there was no overlapping the virtual particle was assumed irreversibly adsorbed at the given position and its coordinates were stored, the number of adsorbed particles N_p is increased by one.

It should be mentioned that particle adsorption at heterogeneous surfaces modeled by spherically shaped sites is a truly three-dimensional process, which contrasts within to adsorption at disk-shaped sites as considered previously [14]. Hence, the adsorbed particle centers are located in various planes and this influences both the adsorption kinetics and the maximum (jamming) coverage of particles.

As usual in the RSA simulation the coverage was calculated as $\Theta_p = \pi a_p^2 N_p$. On the other hand, the dimensionless computer adsorption time is defined as [7,14,15]:

$$\tau = \pi a_p^2 \frac{N_{\text{att}}}{\Delta S} = \pi a_p^2 N_{\text{att}} \quad (1)$$

By plotting Θ_p versus the adsorption time τ defined above one can simulate the kinetics of particle adsorption.

An alternative evaluation of particle adsorption kinetics can be achieved via the available surface function (ASF) approach [14,15]. This function can be defined as normalized probability p of adsorbing a particle for a given configuration of sites, their coverage Θ_s , and the particle coverage Θ_p . Additionally, the ASF is dependent on the particle to site size ratio a_p/a_s denoted by λ . This function can effectively be evaluated from simulations by performing, at fixed Θ_s and Θ_p , a large number of adsorption trials N_{att} and N_{succ} of them being potentially successful. Then, the ASF is defined as the limit of $N_{\text{succ}}/N_{\text{att}}$ when $N_{\text{att}} \rightarrow \infty$. In practice, due to computer time limitations, N_{att} was about 10^5 . Especially important is the value of ASF in the limit of negligible particle coverage denoted by p_0 , since it characterizes the initial flux to heterogeneous

surfaces. This quantity is of a primary interest from the experimental viewpoint. Knowing ASF one can calculate particle adsorption kinetics by integrating the constitutive expression [12–15]:

$$\frac{d\Theta_p}{d\tau} = p \quad (2)$$

As discussed in [16] this classical concept of the ASF may not be general enough to deal with diffusion-controlled adsorption of particles. More refined approaches, considering various transport mechanisms of particles in the bulk have been proposed [17–19]. However, due to insurmountable mathematical problems, their applicability for heterogeneous surface adsorption seems prohibitive. Therefore, in this work, we adopt the standard ASF concept which reflects the most important features of the problem of particle adsorption at heterogeneous surfaces. This function can be used for specifying boundary conditions for the bulk transport equation as shown in [20].

The pair correlation function $g(r)$ (often referred to as the radial distribution function (RDF)) was calculated by generating particle populations according to the above RSA scheme and exploiting the definition [9]:

$$g(r) = \frac{\pi a_p^2}{\Theta_p} \left\langle \frac{\Delta N_p}{2\pi r \Delta r} \right\rangle \quad (3)$$

where $\langle \rangle$ means the ensemble average and ΔN_p is the number of particles adsorbed within the ring $2r\Delta r$ drawn around a central particle. It should be mentioned that the distance r was measured between the projection of the adsorbed particle centers on the adsorption plane. Obviously, all particles located close to the periphery of the simulation area were discarded from the averaging procedure. In order to obtain $g(r)$ with satisfactory accuracy particle populations reaching 10^5 were considered.

3. Results and discussion

3.1. Numerical results

The numerical calculations discussed hereafter, concerning the pair correlation function, the ASF, adsorption kinetics and jamming coverage have been carried out for $\lambda = 2, 5$ and 10 which appear to be typical for practically occurring situations.

Examples of mono-layers generated in simulations are shown in Fig. 2 for $\lambda = 2$, site coverage $\Theta_s = 0.1$ and increasing particle coverage $\Theta_p = 0.1, 0.2$ and 0.5 , respectively. In the latter case, the jamming state

was attained, since no additional particle could be adsorbed at the interface (no available centers left). It is interesting to observe that for conditions corresponding to the jammed state one site can coordinate

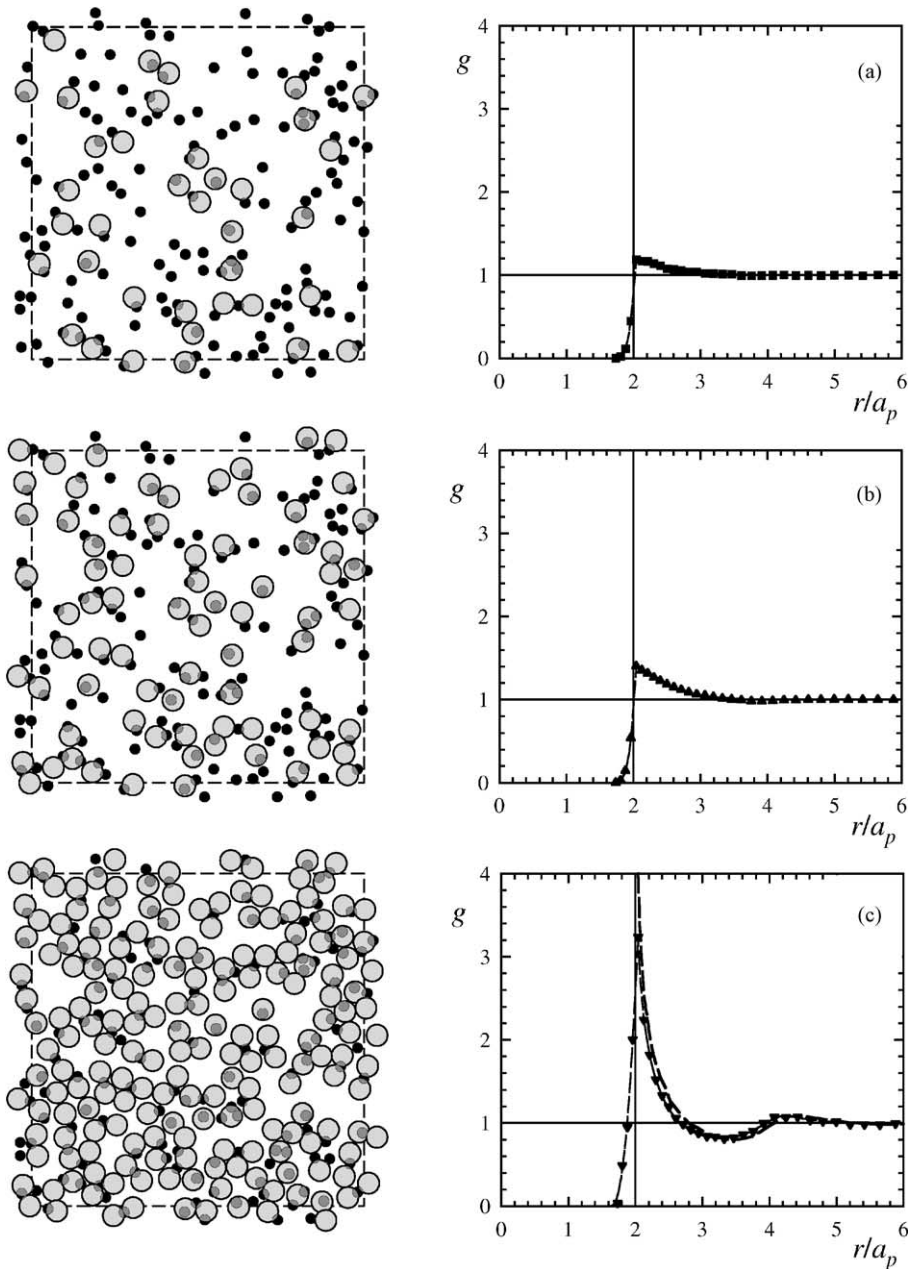


Fig. 2. Particle mono-layers and pair correlation function g derived from numerical simulations for $\lambda = 2$, $\Theta_s = 0.1$ (black circles represent adsorption centers and gray circles represent adsorbed particles). (a) $\Theta_p = 0.1$; (b) $\Theta_p = 0.2$; (c) $\Theta_p = 0.5$ (jamming) the dashed line denotes the results pertinent to uniform surfaces (derived from the standard RSA model).

more than one particle. This indicates that the site multiplicity n_s , which depends in the general case on λ , Θ_s and Θ_p , was larger than one. It should be noted, however, that due to geometrical constants in the case $\lambda > 4$, one center can coordinate only one particle which means that n_s remains always smaller than one.

The structure of particle mono-layers which is of interest in practical applications, can be characterized quantitatively in terms of the pair correlation function $g(r)$. This function was determined from particle populations generated in simulations according to the procedure described above. The distributions of g derived from numerical simulations for various Θ_p are shown in Fig. 2. As can be deduced, at small coverage ($\Theta_p = 0.1$) the particles are almost uniformly distributed, since g remains close to unity for separations $r/a_p < 2$. On the other hand, for higher coverage, a considerable degree of short-range ordering, analogous to a 2D liquid, is observed within the particle mono-layer. In this case, the $g(r)$ function resembles closely, for $r/a_p > 2$, the function derived from RSA simulations for homogeneous surfaces [11]. This prediction, confirming the possibility of producing dense mono-layers characterized by a maximum in the interparticle distance at short separations has implications for colloid lithography. One should notice, however, that the $g(r)$ function remains finite for $r/a_p < 2$. This indicates that in contrast to homogeneous surfaces, adsorption at sites occurs in various planes, so particle projections on the interface can overlap. This is analogous to the behavior predicted theoretically and observed at homogeneous surfaces for polydisperse particle systems [21].

Except for the pair correlation function, the quantity of a primary practical interest is the ASF which represents the averaged probability of adsorbing the particle at an interface covered by a given number of sites and previously adsorbed particles. Hence, by knowing the ASF one can predict the flux of particles to heterogeneous surfaces (adsorption rate). Especially important is the value of the ASF in the limit of $\Theta_p \rightarrow 0$, denoted by p_0 . This quantity characterizes the initial adsorption rate of particles, often referred to as the limiting flux [8]. The dependence of p_0 on Θ_s derived from numerical simulations for $\lambda = 2, 5$ and 10 is plotted in Fig. 3. As can be observed, the adsorption probability of particles increases abruptly with Θ_s , especially for larger λ values. For $\lambda = 10$, the

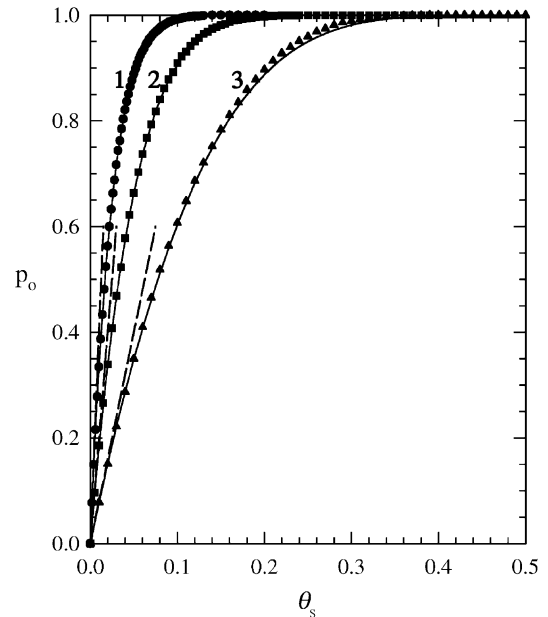


Fig. 3. The dependence of the initial adsorption probability p_0 on the surface coverage of adsorption sites Θ_s ; the points denote numerical simulations performed for (1) (●), $\lambda = 10$; (2) (■), $\lambda = 5$; (3) (▲), $\lambda = 2$; the solid lines represent the analytical results derived from Eq. (4); the broken line represent the analytical results derived from Eq. (5).

probability of adsorption reaches unity (the value pertinent to homogeneous surfaces) for Θ_s as low as 0.1. It is interesting to observe that the numerical data shown in Fig. 3 are well reflected for the entire range of λ and Θ_s by the analytical formula:

$$p_0 = 1 - (1 - \Theta_s) \times \exp\left(\frac{-(4\lambda - 1)\Theta_s}{1 - \Theta_s} - \left[\frac{(2\sqrt{\lambda} - 1)\Theta_s}{1 - \Theta_s}\right]^2\right) \quad (4)$$

Eq. (4) was previously derived [9] by exploiting the scaled particle theory of Reiss et al. [22]. Using the above expression one can predict results for arbitrary λ value. This is important because the numerical simulations are very cumbersome and time consuming.

It is also interesting to note that in the limit $\Theta_s < 1/(4\lambda - 1)$, Eq. (4) simplifies to

$$p_0 = 4\lambda\Theta_s \quad (5)$$

The results shown in Fig. 3 imply also that by measuring experimentally the flux of larger colloid particles (which can easily be done by direct microscope observations as discussed later in the paper) one can detect the presence of nanoscale surface heterogeneities, invisible under the microscope. If the surface concentration of the sites can be estimated one can determine their size from the particle deposition experiments.

One should remember, however, that the results shown in Fig. 3 describe particle adsorption rates at heterogeneous surfaces in the limit when their accumulation is negligible, i.e. for $\Theta_p \rightarrow 0$ only. If Θ_p becomes finite, the probability of particle adsorption decreases due to volume exclusion effects (often referred to less accurately as surface blocking effects). The adsorption probability is then a function of Θ_s , Θ_p and λ . It was found that the theoretical results derived from the simulations can be conveniently expressed as the dependence of the reduced ASF p/p_0 on Θ_p for a fixed Θ . As may be observed in Fig. 4, where such results are plotted ($\lambda = 2$, $\Theta_s = 0.05$), the p/p_0 func-

tion can well reflected for $\Theta_p < 0.1$ by the Langmuir-like model, given by the formula:

$$p = 4\lambda\Theta_s \left(1 - \frac{\Theta_p}{\lambda^2\Theta_s n_s}\right) (1 - 4\Theta_p) \cong p_0 \left(1 - \frac{\Theta_p}{\Theta_p^{\text{mx}}}\right) \tag{6}$$

where

$$\Theta_p^{\text{mx}} = \frac{\lambda^2 n_s \Theta_s}{1 + 4\lambda^2 n_s \Theta_s} \tag{7}$$

can be treated as the apparent saturation coverage.

Eq. (7) was derived in [9] by assuming that particle adsorption probability, in the limit of low particle coverage, is proportional to the number of unoccupied sites and to the available surface area $1 - 4\Theta_p$. The site multiplicity parameter n_s , for $\lambda = 2$, was found from numerical simulations to be 2.45 (in the limit of low coverage Θ_p).

The data showing in Fig. 4, for the higher site coverage ($\Theta_s = 0.2$) demonstrate that the p/p_0 function deviates considerably from the Langmuir model and can well be reflected by the dependence derived from the classical RSA approach [12,13] for homogenous surface adsorption, similar results were obtained for $\lambda = 5$ and 10. One can conclude, therefore, that in the case when $\lambda^2\Theta_s > 1$ particle adsorption on heterogeneous surfaces is governed by the function:

$$p = p_0 B(\Theta_p) \tag{8}$$

with $p_0(\lambda, \Theta)$ given by Eq. (4) and $B(\Theta_p)$ (the surface blocking function) calculated from the standard RSA of uniform surfaces [12,13]:

$$B(\Theta_p) = f(\Theta_p) \left(1 - \frac{\Theta_p}{\Theta_p^\infty}\right)^3 \tag{9}$$

where Θ_p^∞ is the jamming coverage of particles equals 0.547 for homogeneous surfaces and $f(\Theta_p)$ are low-order polynomials. One of the most accurate expressions for $f(\Theta_p)$ has the form [12]:

$$f(\Theta_p) = 1 + 0.812\bar{\Theta}_p + 0.426\bar{\Theta}_p^2 + 0.0716\bar{\Theta}_p^3 \tag{10}$$

where $\bar{\Theta}_p = \Theta_p/\Theta_p^\infty$

Using Eqs. (8)–(10) one can express the constitutive expressions, Eq. (2) in the form:

$$\int^{\Theta_p} \frac{d\Theta'}{B(\Theta')} = \frac{p_0\tau}{\Theta_p^\infty} = \tau' \tag{11}$$

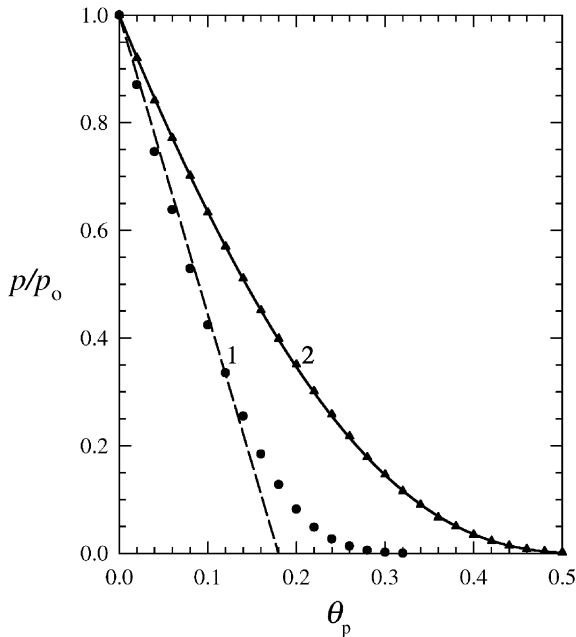


Fig. 4. The dependence of the reduced adsorption probability p/p_0 on Θ_p ; the points denote numerical results obtained for $\lambda = 2$ and (1) $\Theta_s = 0.05$; (2) $\Theta_s = 0.2$; the solid line represents the results for the RSA model (homogeneous surfaces) Eq. (9); the dashed line shows the results predicted from the Langmuir model using Eq. (6).

One can deduce from Eq. (11) that all kinetic results known previously for homogeneous surfaces can be directly transferred to heterogeneous surfaces by introducing the transformed adsorption time $\tau' = p_0(\Theta_s, \lambda) / \Theta_p^\infty$. One should remember, however, that this is true in the limit of higher site density only when the inequality $\lambda^2 \Theta_s > 1$ is met. Because the evaluation of the integral in Eq. (11) is rather awkward, Jin et al. [15] derived the following interpolation function which approximates the integral well:

$$\Theta_p = \Theta_\infty \left(1 - \frac{1 + 0.314\tau'^2 + 0.45\tau'^3}{1 + 1.83\tau' + 0.66\tau'^3 + \tau'^{7/2}} \right) \quad (12)$$

Extensive numerical simulations discussed in [15] confirmed the validity of this formula.

The jamming coverage Θ_p^∞ used for the above time transformation has a fundamental practical significance, since it determines the “capacity” of an interface, i.e. the maximum amount of solute (particles) which can be adsorbed. We have performed, therefore, extensive simulations aimed at determining this parameter as a function of Θ_s and λ . The results plotted as

the dependence of Θ_p^∞ on Θ_s (in logarithmic scale) are reported in Fig. 5. The analytical results predicted in the limit of $\Theta_s \rightarrow 0$ from the formula $\Theta_p = n_s \lambda^2 \Theta_s$ are also plotted for comparison (dashed lines in Fig. 5) and, as may be observed, this analytical formula works well for $\lambda^2 \Theta_s < 0.02$ only. It was found that for higher site coverage the numerical results can be correlated by the simple analytical function:

$$\Theta_p^\infty = \Theta_\infty (1 - e^{-n_s \lambda^2 \Theta_s / \Theta_\infty}) \quad (13)$$

This formula provides satisfactory accuracy for the entire range of Θ_s studied. However, it becomes less accurate for $\lambda = 2$ in the region where a maximum appears (for $\Theta_s = 0.2$). This maximum jamming coverage attains the value of 0.57 which is slightly larger than for adsorption on uniform surfaces. The maximum appears because, for this Θ_s range the area accessible for particle adsorption becomes larger than the geometrical interfacial area. This can be interpreted as apparent roughness effect. When Θ_s increases further above this critical value, the accessible area becomes again very close to the geometrical interfacial area. Although

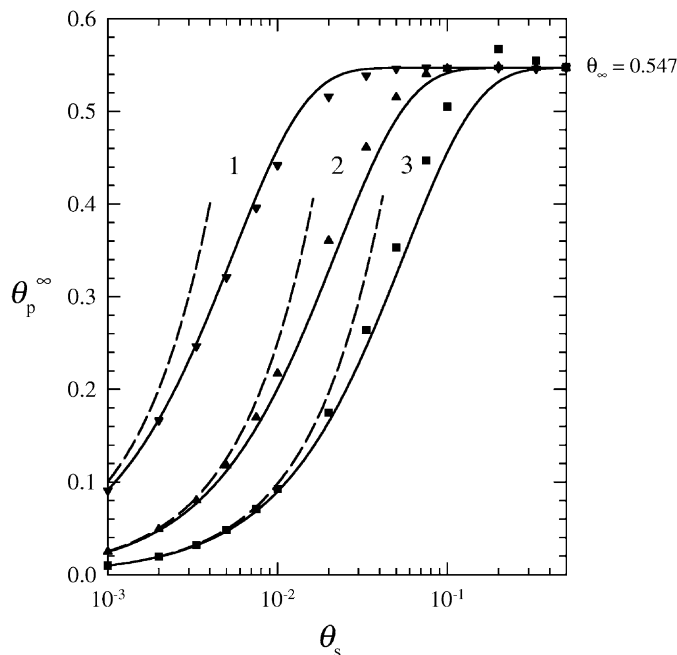


Fig. 5. The dependence of the jamming coverage of particles Θ_p^∞ on the coverage of the adsorption sites Θ_s ; the points denote the results of numerical simulations, performed for (1) (\blacktriangledown), $\lambda = 10$; (2) (\blacktriangle), $\lambda = 5$; (3) (\blacksquare), $\lambda = 2$; the solid lines represent the fitting function given by Eq. (13); the dashed lines show the results calculated from the expression $\Theta_p = n_s \lambda^2 \Theta_s$.

this effect is interesting from a theoretical point of view it does not have significant practical implications. This is so because in practice it is very difficult to measure surface coverages of the particles with a relative accuracy better than 5%, for example due to polydispersity effects [21].

It should be mentioned that all the results obtained in this work concern hard particle adsorption, when the range of interactions is much smaller than the dimensions of the particles. Such a situation may be realized experimentally for high electrolyte concentrations when the electrostatic double-layer interactions are eliminated [8]. For dilute electrolytes the interaction becomes comparable with particle size which affects both adsorption kinetics and the jamming coverage. The latter parameter for interacting systems can be calculated using the effective hard particle concept developed in [7].

3.2. Experimental results

Particle adsorption experiments were carried out using the direct microscope observation method in the impinging-jet cell applied before for similar studies [6–8,10,21]. The cell is shown schematically in Fig. 6. Because of the hydrostatic pressure difference the particle suspension was driven through a circular capillary of the radius $R = 0.073$ cm, impinged against a perpendicularly oriented mica plate, and left the cell through the external tubing. After use, the suspension was discarded. The volumetric flow rate Q in the cell was regulated by the change of the level of the outlet tubing. This allowed one to change the flow Reynolds number $Re = Q/\pi Rv$ within broad limits (where v is the kinematic viscosity of the suspension). Because of the underpressure prevailing in the cell, the mica plate was held fixed to the external tube without using any adhesive which reduced the possibility of cell contamination during the measurements.

Adsorbed particles were observed in situ under an optical microscope (Leitz, Germany, dark-field illumination) coupled with a CCD camera, an image processor and video recorder.

The colloid particles used in the experiments were polystyrene lattices of low polydispersity confined within 5–10%. The negatively charged suspensions were synthesized according to the polymerization procedure described in [23] using a persulfate initiator.

The positively charged latex suspensions (used for modeling adsorption sites) were produced using a similar procedure with the azonitrile initiator. The concentrated stock samples obtained from the polymerization were purified by steam distillation and prolonged membrane filtration according to the procedure described previously [6–8].

Particle size and concentration in the dilute samples used in experiments were determined by the Coulter–Counter method with an accuracy of a few percent. The averaged size of the two negative lattices used in our experiments were 1.38 ± 0.1 and 0.87 ± 0.06 μm . The positive latex particles had an averaged diameter $2a_s$ of 0.55 ± 0.4 μm .

As the adsorbing surface, mica sheets provided by Mica and Micanite Supplies Ltd., England were used. The sheets were freshly cleaved before each experiment and used without any pretreatment. The zeta potential of mica was determined by the streaming potential method in the plane-parallel channel cell [24]. For an ionic strength of 10^{-4} M the potential was found to be -90 mV and for 10^{-4} M the potential was -80 mV.

The experimental procedure was as follows: first the mica surface was covered by positive latex in separate runs carried out at very low Reynolds number and at an ionic strength of 10^{-4} M. By changing the adsorption time and bulk suspension concentration, the desired surface concentration of particles was attained and determined by direct microscope counting over statistically chosen areas. The total number of particles was about 1000–2000, which ensured a relative precision better than 3%. For the sake of convenience the surface concentration of particles was expressed as the dimensionless coverage $\Theta_s = \pi a_s^2 \langle N_s \rangle$ (where $\langle N_s \rangle$ is the average surface concentration of adsorbed smaller particles). In our experiments Θ_s varied between 0 and 0.2.

After preparing the heterogeneous mica surface, the positive latex suspension was replaced in situ by the negative latex suspension of a given bulk concentration n_b which varied usually between 2×10^8 and 8×10^8 cm^{-3} . The adsorption kinetics were subsequently followed by determining the averaged surface concentration $\langle N_p \rangle$ of larger particles as a function of time. To obtain a single point on the kinetic curve, 100–500 particles were counted over statistically chosen areas having typical dimensions of 100 per 100 μm . All these areas were located not further than

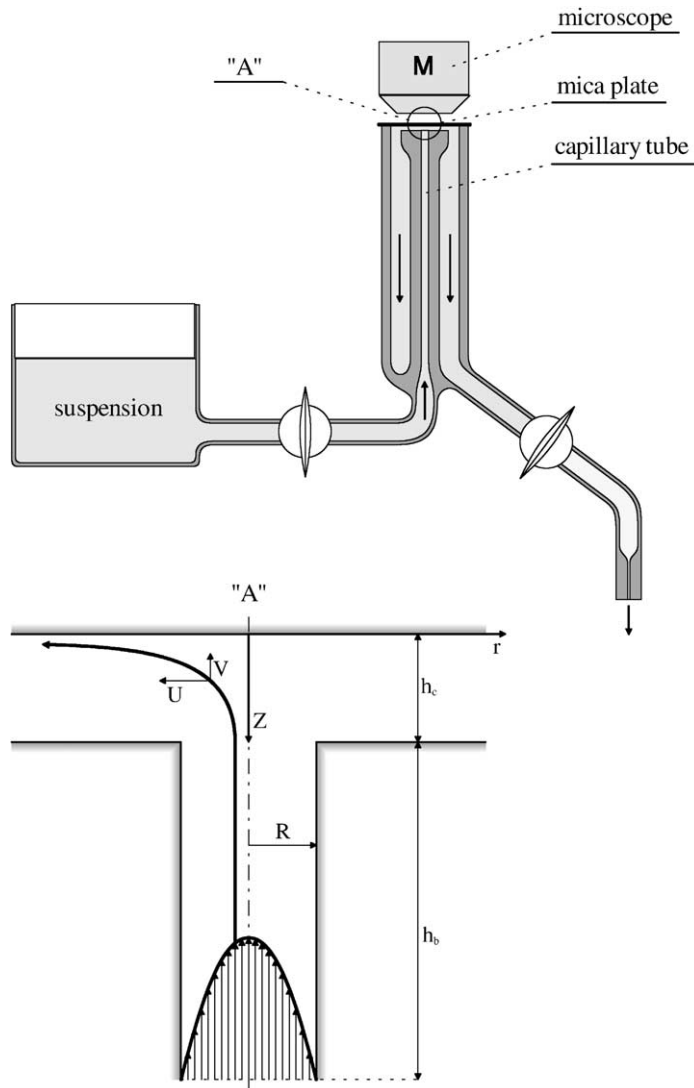


Fig. 6. The experimental cell used for measurements of particle adsorption.

200 μm from the stagnation point (center of the cell) where the interface remains uniformly accessible for particle transport [8]. The dimensionless surface coverage of the larger particles was calculated as $\Theta_p = \pi a_p^2 \langle N_p \rangle$.

The kinetic runs were fitted by linear or parabolic regression lines (in the case of higher coverage) whose slope at $t \rightarrow 0$ gave the initial flux values for a given coverage of smaller particles.

It was proven in separate experiments that up to the maximum Reynolds number studied particle adsorp-

tion was perfectly irreversible and localized. No lateral motion or particle desorption was observed for experimental times reaching 24 h.

4. Results and discussion

In a series of preliminary experiments it was proven that no measurable deposition of larger particles was observed in the case of bare mica and larger particle adsorption occurred only if $\Theta_s > 0$. A micrograph of a

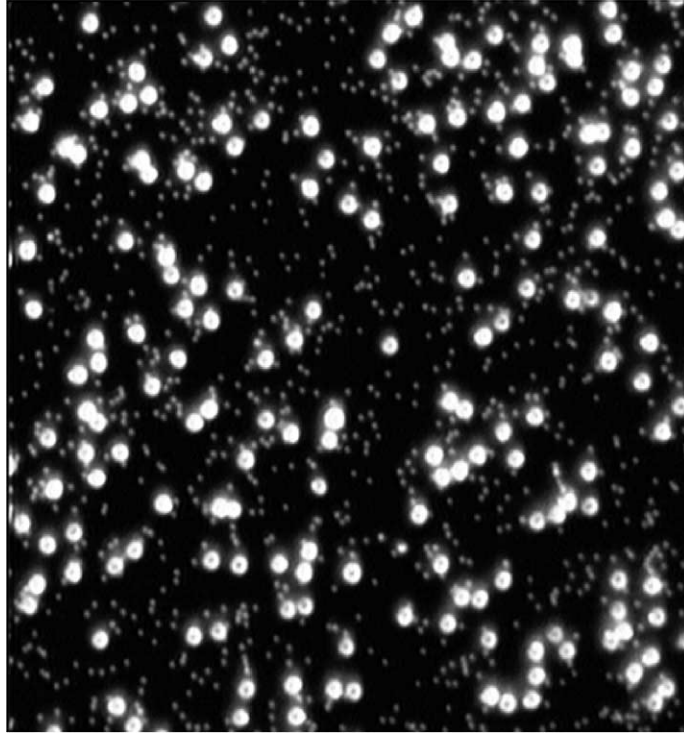


Fig. 7. A micrograph of polystyrene latex particles (diameter 1.38 μm) adsorbed on mica pre-covered by smaller latex particles (adsorption sites) of diameter 0.55 μm , $Re = 2$, $I = 10^{-4}$ M, $\lambda = 2.5$, $\Theta_s = \Theta_p = 0.04$.

typical mono-layer obtained in our experiments ($\Theta_s = 0.04$, $\Theta_p = 0.04$) is shown in Fig. 7. Note that both the smaller and larger particles can be directly seen at the interface, which enables a quantitative analysis of particle distribution and adsorption kinetics. It was proven by a thorough variance analysis that particle distributions were uniform with no tendency to clustering as is often the case for mono-layers dried before microscope observation.

Some typical kinetic runs determined for initial stages of adsorption and $\Theta_s = 0.018$, 0.026 ($Re = 2$, $I = 10^{-4}$ M, $2a_p = 1.38$, $\lambda = 2.5$) are shown in Fig. 8. As one may observe, the dependence of the larger particle coverage Θ_p on adsorption time t remains linear with the slope increasing with the coverage of active centers (smaller particles). For comparison the limiting theoretical results predicted for a uniform surface are also plotted in Fig. 8 (the dash lines). These results have been obtained by a numerical solution of the governing mass transfer equation according to the procedure discussed extensively elsewhere [6,25]. As

can be observed in Fig. 8, for Θ_s as low as a few percent, the particle adsorption rate on heterogeneous surfaces attains the limiting value pertinent to homogeneous surfaces.

From the linear kinetic runs shown in Fig. 8 one can calculate the initial flux of particles (initial adsorption rate) using the definition:

$$|j_0(\Theta_s)| = \frac{1}{\pi a_p^2} \frac{\Delta\Theta_p}{\Delta t} \quad (14)$$

where $\Delta\Theta_p/\Delta t$ is the slope obtained by linear regression of the experimental data.

It was also found in separate runs that the initial flux was proportional to the bulk suspension concentration n_b which indicates that the larger particle adsorption was indeed a linear process for the range of times studied (reaching 30 min). This fact enabled us to increase the accuracy of measurement of the initial flux, since averages from many kinetic runs performed for various n_b could be taken. It is, therefore, advantageous to express the initial flux in the reduced form

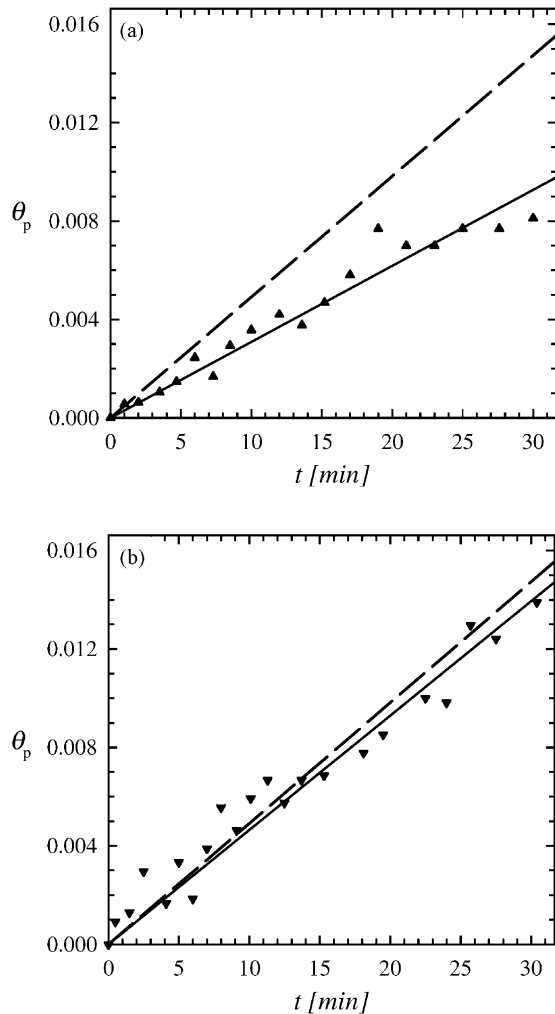


Fig. 8. Initial kinetics of latex particle adsorption on mica covered by adsorption sites determined experimentally for $Re = 2$, $I = 10^{-4}$ M, $\lambda = 2.5$. (a) $\Theta_s = 0.018$; (b) $\Theta_s = 0.026$; continuous lines denote the linear fits; the dashed lines represent the theoretical results predicted for homogeneous surfaces.

$j_0(\Theta_s)/n_b = k_0(\Theta_s)$, where $k_0(\Theta_s)$ is the mass transfer rate constant. We determined experimentally the dependence of the reduced flux on the site coverage Θ_s . It was found that the flux approached 2.04×10^{-6} cm/s for $\Theta_s = 0.2$. This is close to the theoretical value pertinent to uniform surfaces $j/n_b = k_b$, equal 1.92×10^{-6} cm/s, (where k_b is the reduced flux to a uniform surface). This limiting flux, denoted by j_{mx} is an important parameter because it can be used as a scaling variable for expressing the

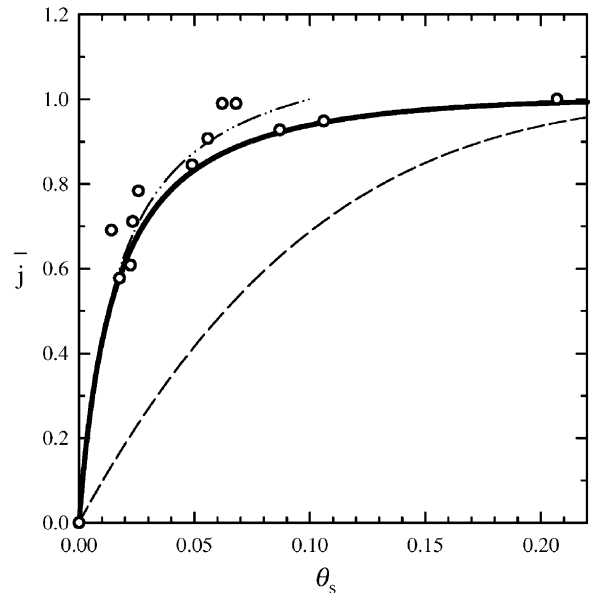


Fig. 9. The dependence of the scaled flux $\bar{j} = j_0(\Theta_s)/j_{mx}$ on Θ_s . The points denote the experimental results obtained for $Re = 2$, $I = 10^{-4}$ M, $\lambda = 2.5$, the solid line represents the theoretical results derived from Eq. (15) for $K = 7$, the dashed line shows the results obtained from Eq. (15) for $K = 1$ and the dash-dotted line shows the results calculated from Eq. (16).

experimental dependence of the flux on site coverage. This form of presentation of the results is advantageous for their theoretical analysis. In Fig. 9 the experimentally determined dependence of the scaled flux $\bar{j} = j_0(\Theta_s)/j_{mx}$ on Θ_s is plotted. As can be observed the scaled flux increases abruptly with Θ_s , approaching the limiting values for Θ_s of a few percent. These experimental data suggest that the kinetics of particle adsorption on heterogeneous surfaces during the initial stages when the surface coverage remains low can well be predicted by the convective theory elaborated for uniform surfaces [8]. This has a practical significance since many known theoretical and experimental data for uniform surfaces can directly be transferred to heterogeneous system adsorption.

A quantitative interpretation of these results can be attained by exploiting the above theoretical predictions, expressed by Eq. (4) which describes particle transfer through the surface layer at low colloidal particle coverages. By coupling this equations with the bulk transport of particles governed by convective

diffusion one can derive the following relationship [9]:

$$\bar{j} = \frac{K \langle p(\Theta_s, \Theta_p) \rangle}{1 + (K - 1) \langle p(\Theta_s, \Theta_p) \rangle} = \frac{1}{\pi a^2 j_{\text{mx}}} \frac{d\Theta_p}{dt} \quad (15)$$

where $K = k_a/k_b$, $\langle p(\Theta_s, \Theta_p) \rangle$ is the integrated probability (generalized blocking function [18]) and k_a is the adsorption rate constant calculated as [9,10]:

$$k_a = \int_{\delta_m}^{\delta_a} \frac{e^{\phi/kT}}{D(h)} dh$$

where δ_m is the minimum distance between the particle and the interface, δ_a is the adsorption layer thickness, ϕ is the interaction energy of the particle with the interface, k is the Boltzmann constant, T the absolute temperature and D is the particle diffusion coefficient which depends on the distance from the interface h .

Due to mathematical limitations $\langle p(\Theta_s, \Theta_s) \rangle$ has been calculated explicitly only for a limited range of coverage in the case of adsorption over uniform interfaces [18]. However, it was demonstrated in [26] that for practical applications, when only moderate accuracy is required, the integrated probability can be well approximated by the function $p(\Theta_s, \Theta_p)$ discussed above. Assuming this, one can apply Eq. (15) with $p(\Theta_s, \Theta_p)$ given by Eq. (4) to describe particle flux to heterogeneous surfaces. A useful analytical expression can be derived if $\lambda\Theta_s \ll 1$ when Eq. (5) applies. Then, Eq. (15) can be expressed as:

$$\bar{j} = \frac{4\lambda K \Theta_s}{1 + 4\lambda(K - 1)\Theta_s} \quad (16)$$

The theoretical results stemming from the above approach are compared with experimental results in Fig. 9. The relevant parameters for our experimental conditions were $\lambda = 2.5$ (particle size ratio) and $K_a = 7$. The latter value was calculated by assuming that the thickness of the adsorption layer δ_a was equal to the diameter of smaller particles (heterogeneities) and taking $k_b = 2.04 \times 10^{-6}$ cm/s, i.e. equal to the experimentally determined value for large Θ_s . As one can observe in Fig. 9, the experimental results are quantitatively reflected by Eq. (15) for the entire range of smaller particle coverage Θ_s . As expected, Eq. (16) gives also a satisfactory agreement with the experimental data for $\Theta_s < 0.1$. These facts suggest that the basic features of particle adsorption on heterogeneous surfaces are well reflected by these equations and this

has a considerable practical significance in view of its simplicity. In particular, one can deduce from Eq. (16) that the flux for heterogeneous surfaces attains the limiting value for uniform surfaces for the critical value of Θ_s given by:

$$\Theta_s > \frac{1}{4\lambda K} = \frac{a_s k_b}{4a_p k_a} \quad (17)$$

Since, this limiting value is proportional to a_s and k_b , one can expect that the increase in the flux should be most dramatic for small heterogeneity size and low flow rate (Reynolds number) when the thickness of the diffusion boundary layer becomes significantly larger than particle dimensions.

The above experimental data, however, are only concerned with the initial adsorption stages when particle accumulation at the surface remains negligible. For higher coverages a significant deviation of the adsorption kinetics from linearity occurs as a result of blocking effects. This is clearly demonstrated in Fig. 10 where the experimental results obtained for

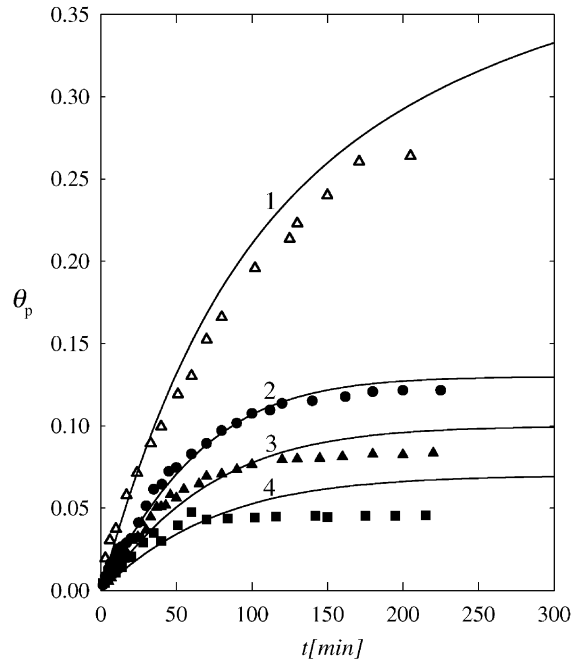


Fig. 10. Adsorption kinetics on heterogeneous surfaces determined for $Re = 2$, $I = 10^{-3}$ M, $\lambda = 1.6$, the points denote experimental results obtained for (1) (Δ), $\Theta_s = 0.18$; (2) (\bullet), $\Theta_s = 0.042$; (3) (\blacktriangle), $\Theta_s = 0.026$; (4) (\blacksquare), $\Theta_s = 0.016$; the solid lines represent the theoretical results calculated from Eqs. (12) and (18) (for curve no. 1).

($Re = 2$, $I = 10^{-4}$ M, $2a_p = 0.87$, $\lambda = 1.6$) are plotted. In this series of experiments the smaller particle to heterogeneity size ratio was chosen because this allowed one to measure more accurately the kinetics for higher particle coverage. The aim of these experiments was to test the validity of the theoretical results to predict not only the initial flux but also the kinetics within the non-linear adsorption regime. The theoretical predictions can be derived by integrating Eq. (15) with respect to time to provide the expression:

$$(K - 1)\Theta_p + \int_0^{\Theta_p} \frac{d\Theta'}{\langle p(\Theta_s, \Theta') \rangle} = K\pi a^2 j_{\text{mx}} n_b t \quad (18)$$

For moderate to high site coverage, using Eq. (6) to approximate the integrated adsorption probability, one can express Eq. (18) explicitly as:

$$\Theta_p = \Theta_p^{\text{mx}} \left[1 - \exp\left(\frac{-4\lambda\Theta_s}{\Theta_p^{\text{mx}}} (K\pi a^2 n_b t)\right) \right] \quad (19)$$

where Θ_p^{mx} is the apparent saturation coverage given by Eq. (7). The site multiplicity parameter was taken from the numerical simulations. On the other hand, the constant K was found to be 3.2 for the experimental conditions ($k_b = 8.9 \times 10^{-9}$ cm/s, $k_a = 2.9 \times 10^{-6}$ cm/s). As one can observe in Fig. 10 the theoretical results derived from Eq. (19) describe quite satisfactorily the experimental kinetic runs. The slight deviation appearing at longer adsorption times and $\Theta_s = 0.016$ can be probably attributed to the finite value of the binding energy between the particle and the site. As a result, a small fraction of sites may prove to be inactive in the immobilization process of the particles. The agreement of the experimental data with Eq. (19) indicates that for low site density ($\Theta_s < 0.05$) particle adsorption can be well described by the pseudo Langmuirian model. On the other hand, as can be observed in Fig. 10, for high site coverage, $\Theta_s = 0.18$, particle adsorption is well described by the classical RSA model. In this case, the particle adsorption on heterogeneous surfaces approaches the limiting adsorption regime pertinent to uniform surfaces not only for the initial stages but for the entire range of times. This conclusion, which was important practical implications, is further confirmed by the collection of experimental data plotted in Fig. 11. As can be seen,

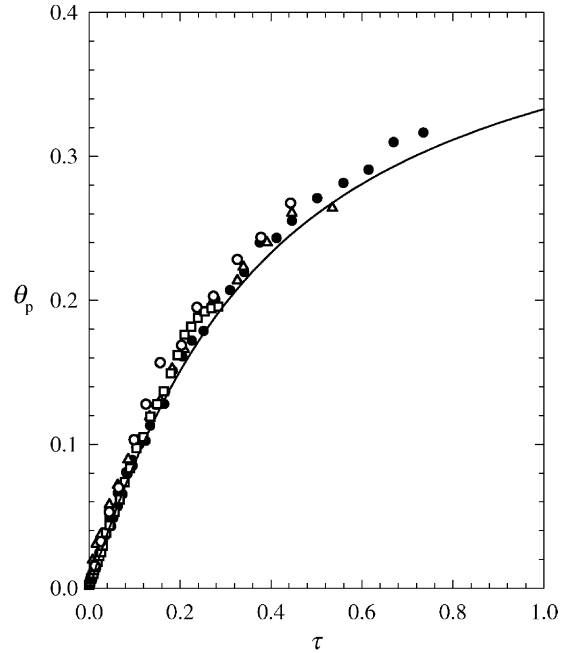


Fig. 11. Adsorption kinetics on heterogeneous surfaces expressed in terms of the reduced adsorption time $\tau = \pi a^2 k_b n_b t$; the points denote experimental results obtained for various adsorption sites, i.e. latex particles, colloid iron oxide, colloid aluminum hydroxide. The solid line denotes the theoretical results predicted by the RSA model, Eq. (12).

experimental data obtained for various λ values and morphologies of the adsorption sites (either polystyrene latex, or inorganic colloid particles) collapse onto a universal curve by introducing the reduced time $\tau = t/t_{\text{ch}}$ (where $t_{\text{ch}} = \pi a^2 j_{\text{mx}}$). This is fully in agreement with the theoretical prediction expressed by Eq. (11).

4.1. Concluding remarks

It was predicted theoretically that adsorption probability on heterogeneous surfaces can be described for low site densities, $\Theta_s < 1/4\lambda$, by the pseudo-Langmuir model:

$$p = 4\lambda\Theta_s \left(1 - \frac{\Theta_p}{\Theta_p^{\text{mx}}} \right)$$

where the apparent saturation coverage Θ_p^{mx} is given by Eq. (9).

On the other hand, for high site density, when $\lambda^2\theta_s > 1$, the particle adsorption probability is described by the formula:

$$p = p_0 B(\theta_p)$$

where $B(\theta_p)$ is the blocking function derived from the standard RSA model for uniform surfaces. This indicates that all results known previously for homogeneous surfaces can be directly transferred to heterogeneous surfaces by an appropriate time transformation. In particular one can deduce that the adsorption kinetics is given by Eq. (12) with the reduced adsorption time $\tau' = p_0\tau/\theta_p^\infty$. The jamming coverage θ_p^∞ needed in this transformation can be calculated from the simple interpolating function:

$$\theta_p^\infty = \theta_\infty (1 - e^{-n_s \lambda^2 \theta_s / \theta_\infty})$$

The experiments performed for model colloids confirmed the theoretical predictions, in particular the abrupt increase in adsorption flux with site coverage. This can be attributed to the combined effect of geometrical interception, proportional to $4\lambda\theta_s$ and the coupling with the bulk transport, described by the K parameter. Thus, when the critical value of $\theta_s = 1/4\lambda K$ is exceeded, the kinetics of particle adsorption on a heterogeneous surface (in the initial stages) is well predicted by the convective-diffusion theory derived for a uniform surface.

It was also experimentally proven, using adsorption sites of various morphology, that for higher site densities, particle adsorption kinetics for the entire range of time is described by the standard RSA model formulated for uniform surfaces.

Acknowledgements

This work was supported by KBN Grant 3T09A 105 18.

References

- [1] M.Y. Boluk, T.G.M. van de Ven, *Colloids Surf. A* 46 (1990) 157.
- [2] B. Alinec, T.G.M. van de Ven, *Colloids Surf. A* 71 (1993) 105.
- [3] H.A. Chase, *Chem. Eng. Sci.* 39 (1984) 1099.
- [4] J.M. Peula, R. Hidalgo-Alvarez, F.J.D. de las Nieves, *J. Colloid Interface Sci.* 201 (1998) 139.
- [5] J.A. Molina-Bolivar, F. Galisteo-Gonzalez, R. Hidalgo-Alvarez, *Langmuir* 17 (2001) 2514.
- [6] Z. Adamczyk, M. Zembala, B. Siwek, J. Czarnecki, *J. Colloid Interface Sci.* 110 (1986) 188.
- [7] Z. Adamczyk, M. Zembala, B. Siwek, P. Warszyński, *J. Colloid Interface Sci.* 140 (1990) 123.
- [8] Z. Adamczyk, B. Siwek, M. Zembala, P. Belouschek, *Adv. Colloid Interface Sci.* 48 (1994) 151.
- [9] Z. Adamczyk, P. Weroński, E. Musiał, *J. Colloid Interface Sci.*, in press.
- [10] Z. Adamczyk, B. Siwek, E. Musiał, *Langmuir* 17 (2001) 4529.
- [11] E.L. Hinrichsen, J. Feder, T. Jossang, *J. Statist. Phys.* 44 (1986) 793.
- [12] P. Schaaf, J. Talbot, *J. Chem. Phys.* 91 (1989) 4401.
- [13] B. Senger, J.C. Voegel, P. Schaaf, *Colloids Surf. A* 165 (2000) 255.
- [14] Z. Adamczyk, P. Weroński, E. Musiał, *J. Chem. Phys.*, in press.
- [15] X. Jin, J. Talbot, N.H.L. Wang, *AIChE J.* 40 (1994) 1685.
- [16] B. Senger, P. Schaaf, J.C. Voegel, A. Johnner, A. Schmitt, J. Talbot, *J. Chem. Phys.* 97 (1992) 3813.
- [17] P. Wojtaszczyk, J. Bonet Avalos, J.M. Rubi, *Europhys. Lett.* 40 (1997) 299.
- [18] Z. Adamczyk, B. Senger, J.C. Voegel, P. Schaaf, *J. Chem. Phys.* 110 (1999) 3118.
- [19] J. Faraudo, J. Bafaluy, *J. Chem. Phys.* 112 (2000) 2003.
- [20] Z. Adamczyk, *J. Colloid Interface Sci.* 229 (2000) 477.
- [21] Z. Adamczyk, B. Siwek, M. Zembala, P. Weroński, *J. Colloid Interface Sci.* 185 (1997) 236.
- [22] H. Reiss, H.L. Frisch, J.L. Lebowitz, *J. Chem. Phys.* 31 (1959) 369.
- [23] J.W. Goodwin, J. Hearn, C.C. Ho, R.H. Ottewill, *Colloid Polym. Sci.* 252 (1974) 464.
- [24] M. Zembala, Z. Adamczyk, *Langmuir* 16 (2000) 1593.
- [25] Z. Adamczyk, P. Warszyński, L. Szyk-Warszyńska, P. Weroński, *Colloids Surf. A* 165 (2000) 157.
- [26] Z. Adamczyk, P. Weroński, *Adv. Colloid Interface Sci.* 83 (1999) 137.